Desalination and Water Treatment
www.deswater.com

doi: 10.1080/19443994.2016.1184186

57 (2016) 28042–28055
December

Taylor & Francis
Taylor & Francis Group

Batch and column removal of the dye blue 3R over pumice

Beyhan Kocadagistan, Erdem Kocadagistan*

Engineering Faculty, Environmental Engineering Department, Ataturk University, 25240 Erzurum, Turkey, Tel. +90 442 2314813; email: beyhank@atauni.edu.tr (B. Kocadagistan), Tel. +90 442 2314808; email: myecem@atauni.edu.tr (E. Kocadagistan)

Received 21 July 2014; Accepted 25 April 2016

ABSTRACT

Removal of blue 3R dye (B3R) from wastewaters over pumice has been carried out in batch and fixed-bed column modes. Pumice is a cheap and readily available construction material. In the batch mode of the present study, various essential factors, influencing the adsorption such as dye concentration, amount of adsorbent, pH of the solution and temperature, have been monitored. Attempts have also been made to verify Langmuir, Freundlich and Temkin isotherm models. Langmuir was found to be more favourable in the present study. Maximum adsorbate uptake capacity (q_m) was found 97.58 mg/g for 1 g of pumice at the temperature of 40°C with a highest correlation coefficient of R^2 (0.994). Batch mode kinetic study results showed that the pseudo-second-order kinetic model is dominant during the adsorption. In the continuous mode of the present study, various bed depths, flow rates and dye solution concentration were applied to the adsorption column. Thomas and Clark models have also been tested. Error analysis methods such as sum of square error, sum of absolute error, average relative error and average relative standard error were examined to verify the degree of matching of the column adsorption models to the experimental data. According to the batch and column results of this research, an adsorption column filled with pumice can be accepted a good alternative for the removal of B3R dye from wastewaters.

Keywords: Blue 3R; Adsorption; Batch mode; Column mode

1. Introduction

From the beginning of industrial revolution, the consumption of dyes has gradually increased in many industries such as paper, food, plastic and textile. Therefore, untreated wastewaters of such industries may be an important risk-increasing factor for the pollution of the receiving environment. Due to the toxicological and esthetical reasons, dyes are one of the most important undesired parameters among all the contaminants that existed in industrial sewage [1]. Textile dyes are generally synthetic and molecular structures of them are usually complex aromatic. These type of industrial effluents can be carcinogens and toxic to aquatic life. Some type of these dyes in wastewater can also break down into aromatic amines and cause fatal health problems to human beings and other animals [2]. The components of dyes are generally deeply coloured, complex in structure and stable organic compounds and therefore do not readily degrade in the natural environment [3,4]. These substances can reduce light penetration and affects photosynthesis [5,6].

*Corresponding author.

Various treatment methods have been applied to remove dyes from wastewaters such as membrane process [7], adsorption [8] or combined of membrane and adsorption [9], UV [10], ozonation [11], oxidation [12] and electrolysis [13]. Adsorption is the most favoured method to remove textile dyes from wastewaters due to its higher removal efficiencies but lower costs [14,15].

Adsorbent type is an important parameter of the adsorption processes. Higher surface area, suitable chemical properties, lower cost, commonness and higher adsorption capacities are the preferred adsorbent specifications for the adsorption process.

In recent years, a great number of textile dye removal researches performed with adsorption technique have been published in the literature. Many kinds of adsorbents such as anionic or cationic exchange membranes [16,17], activated clay [18], bentonite [19], pine sawdust [20], resin adsorbents [21], chitosan beads [22], Indian Rosewood sawdust [23], hen feather [24] and jackfruit leaf powder [25] have been used in these researches.

Pumice, the adsorbent material of this study, is a cheap and readily available material having an extensive usage in many industrial or daily life areas such as light concrete aggregate in construction sector, cloth-grinding agent in textile industry, additive material in chemistry and water retainer in agriculture. Researchers have been used it as radiation shielding agent [26], reinforced concrete admixture material [27], hardness removal agent for water [28] or as an adsorbent to remove some important pollutants from water and wastewaters such as uranium and thorium [29], Cu(II) [30], Cr(III) and Cr(VI) [31], phosphorous [32], fluoride [33].

Only a few dye adsorption studies, using pumice stone, have reported by researchers [34,35]. Furthermore, they have carried out these studies in batch adsorption mode. To the best of our knowledge, no other research group has done any work with a pumice-filled column to remove dye from wastewater. To meet this literature deficit, batch and continuous (column) modes were carried out consecutively in the present study.

2. Materials and methods

2.1. Preparation of dye solutions

The adsorbate of the present research is Reactive B3R textile dye. Chemical structure of this dye is given in Fig. 1. Stock solutions of B3R dye was prepared by dissolving 1.0 g of dye in 1,000 mL of distilled water. The experimental solutions were diluted to needed concentrations in the range between 10 and 200 mg/L. Dye concentrations were measured at 570 nm wavelength by Shimadzu UV 160 A model spectrophotometer through the experiments.

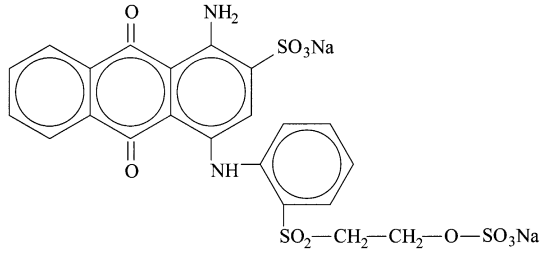

Fig. 1. Chemical structure of B3R dye [36].

2.2. Preparation of pumice

Firstly, pumice stone was grinded and washed with distilled water and dried in an oven for one hour at 105°C. After then, it was sieved to 0.1–0.2 mm mesh range and washed again with 1:2 (w/v) hydrochloric acid solution for 24 h to remove the impurities of pumice and obtain more activated surface. At the end of this process, particles were washed with distilled water several times and dried again. SEM pictures of pumice are given in Fig. 2 and surface area and pore characteristics of pumice are given in Table 1.

2.3. Kinetic and equilibrium studies

The batch adsorption studies were performed at constant shaking speed of 200 rpm. Temperatures were adjusted in the range between 25 and 45°C using a heat adjustable shaker. Batch mode experiments were carried out in 250 mL stoppered glass Erlenmeyer flasks. Adsorbent (pumice) and adsorbate (B3R) were added to the flasks in the range of 1–10 g and 10–100 mg/L, respectively. The pH values of the mixture were measured with WTW Multi 340i model multiparameter device.

The equilibrium adsorption capacity of pumice was calculated by the following equation:

$$q_e = \frac{V(C_o - C_e)}{m} \quad (1)$$

Here, q_e is the equilibrium adsorption capacity of pumice (mg/g), V is the volume of solution (L), C_o and C_e are the concentrations of B3R (mg/L) at initial and any time t, respectively, and m is the dry weight of pumice (g).

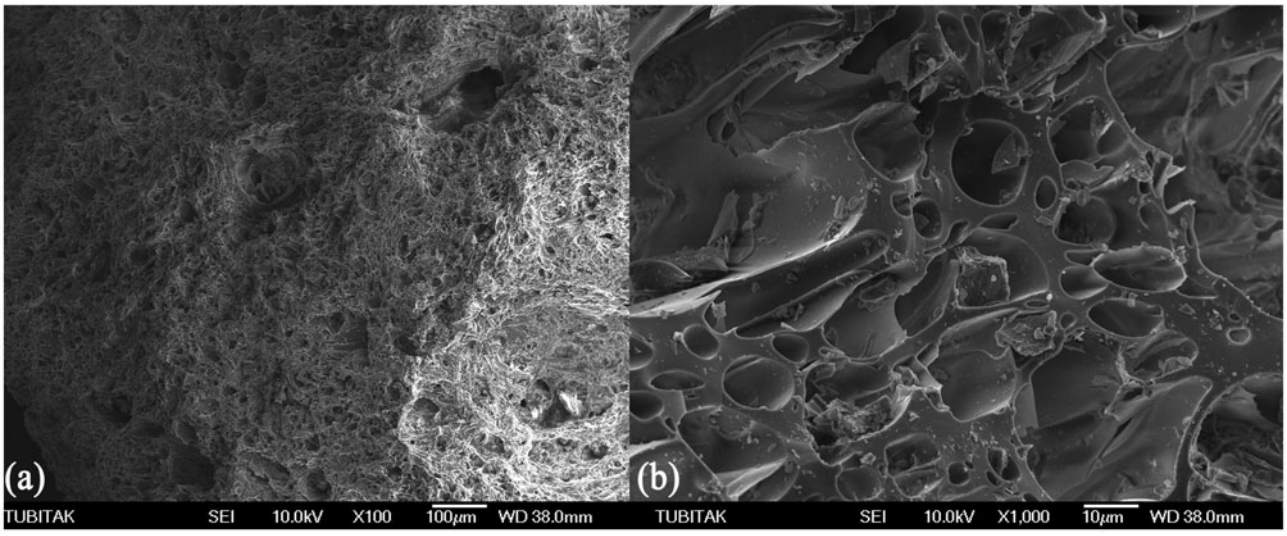

Fig. 2. SEM pictures of pumice (upsizing: a = 100×, b = 1,000×).

Table 1
Surface area and pore characteristics of pumice

BET surface area (m^2/g)	Micropore surface area (m^2/g)	Total pore volume (cm^3/g)	Average pore size (nm)
1.2704	0.958	0.00485	15.2803

2.4. Continuous mode studies

Continuous mode adsorption studies were carried out in a fixed-bed jacketed fibreglass column with an inner diameter of 2.5 cm and a height of 20 cm. To supply upward flow conditions, B3R solutions (in the range of 10–200 mg dye/L) were pumped from the bottom of the column by the aid of a peristaltic pump. Sintered glass filters were placed to inlet and outlet ports to prevent the pumice particles outflow from the column. Samples were collected at equal time intervals from the beginning of experiments to the equilibrium time.

3. Results and discussion

The adsorption study of B3R dye on to the pumice stone was performed in batch and continuous flow operation modes. In batch mode, kinetic and equilibrium evaluations were carried out. After then, continuous flow mode studies were started using a fixed-bed jacketed fibre-glass column to evaluate the breakthrough curves at different operating conditions and to investigate the usability of pumice as an adsorbent in real applications.

3.1. Batch mode studies

To optimize the important process parameters such as biosorbent dose, contact time, pH, dye concentration and temperature for the removal of B3R dye, experiments were carried out using batch procedure at the first period of the study.

3.1.1. Zeta potential measurements

Zeta potential of pumice stones solutions were measured with Zeta-Meter 3.0+ model device. According to the obtained data, the zeta potential values of pumice particles were detected more negative with increasing pH values and reached a maximum value of −38.3 mV at pH 11.70. At about pH 2.60, the zeta potential value was 0 mV (isoelectric point). Therefore, the pH of the B3R solutions was set to 12 ± 0.3 later on the experiments.

3.1.2. Effect of initial B3R concentration and temperature

The adsorption experiments were carried out with different B3R concentrations in the range of

10–100 mg/L at the fixed pH of 12. Fig. 3 shows the effect of initial B3R concentrations on the dye removal efficiencies for 1 g of pumice concentration at 25, 30, 35, 40 and 45°C. As can be seen from this figure, the amount of dye adsorbed increased with increasing initial concentration of B3R dye. This can be explained by the fact that the increasing of the initial dye concentration enhances the interaction between the dye and adsorbent, and it provides the necessary driving force to overcome the resistance to mass transfer between the aqueous and the solid phase [37]. Fig. 3 also shows the temperature effect on adsorption efficiency. The results indicated that the amount of B3R adsorbed and adsorption efficiency increased with increasing temperature up to 40°C. Because the weakening of bonds between dye molecules and binding sites of pumice at higher temperatures, smaller values are observed at 45°C.

3.1.3. Effect of pumice dosage

Fig. 4 shows the effect of adsorbent dose on the amount of dye adsorbed for all working dye concentrations at 40°C. The effect of pumice dose on the adsorption of B3R dye was evaluated by varying the adsorbent doses in the range of 1–10 g. As seen from Fig. 4, for all initial dye concentrations, dye adsorption amounts decreased when the adsorbent dose increased.

3.1.4. Adsorption isotherms

Establish a correlation for the equilibrium curves obtained from the experimental data is essential to optimize the system design of B3R adsorption on to the pumice stone. Therefore, some popular isotherm

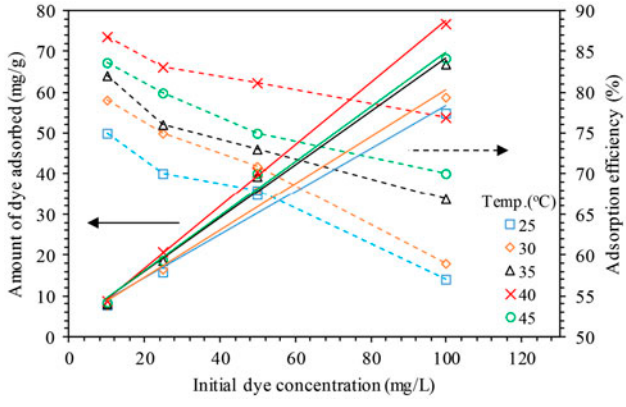

Fig. 3. Effect of initial B3R concentrations on the adsorption capacity (m = 1 g).

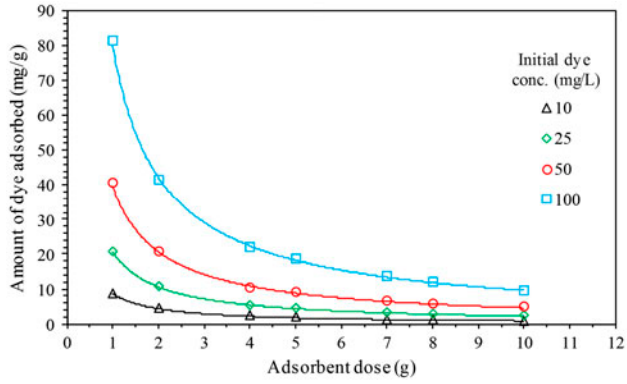

Fig. 4. Effect of adsorbent dose on the adsorption capacity (temperature = 40°C).

models such as Langmuir, Freundlich and Temkin were used in this study.

The Langmuir isotherm in the non-linear form is given as [38]:

$$q_e = \frac{bq_m C_e}{1 + bC_e} \tag{2}$$

According to Eq. (2), the linear form of the Langmuir isotherm can be written as:

$$\frac{1}{q_e} = \frac{1}{q_m b C_e} + \frac{1}{q_m} \tag{3}$$

where q_m is the maximum adsorbate uptake capacity (mg/g) and b is the Langmuir constant related to the energy of adsorption (L/mg).

The non-linear and liner forms of the Freundlich isotherm are commonly presented as [39]:

$$q_e = K_F C^{1/n} \tag{4}$$

and the linear form is:

$$\log q_e = \log K_F + \frac{1}{n} \log C_e \tag{5}$$

where K_F is the constant related to the adsorption capacity, and $1/n$ is the empirical parameter related to the adsorption intensity, which varies with the heterogeneity of the adsorbent material. n, also suggests the affinity of the process (if $n < 1$, chemisorption or $n > 1$, physisorption) [40].

The Temkin isotherm model assumes that the adsorption heat of all molecules in the layer decreases

linearly with coverage at moderate concentrations. Isotherm model is the following [41]:

$$q_e = B \ln(AC_e) \quad (6)$$

and

$$B = RT/b_T \quad (7)$$

where A (L/mg) represents the equilibrium binding constant and B (J/mol) related to the heat of sorption, R is the universal gas constant (8.314 J/mol K), T is the temperature in Kelvin and b_T is the Temkin isotherm constant.

Since the temperature is an important factor on the adsorption process for dye removal [41], isotherm studies were performed at different temperatures in the range of 25–45˚C.

The entire isotherm parameters are given in Table 2. As can be seen from this table, Langmuir isotherm can be accepted more appropriate for modelling of the B3R adsorption equilibrium onto pumice. The q_m values were increased with increasing temperature up to 40˚C but decreased with increasing adsorbent quantities at all working temperatures. On the other hand, R^2 values of Langmuir, Freundlich and Temkin adsorption isotherm models were observed as maximum at the temperature of 40˚C in the present study. Dye removal efficiencies, obtained from the batch studies, showed similar runs. To make the results more interpretively, these efficiencies were given all together in Fig. 5. As seen from this figure, dye removal efficiencies, are increased with increasing temperature up to 40˚C and then decreased slowly. This can be explained by the weakening of bonds between dye molecules and binding sites of pumice at higher temperatures and indicated the exothermic nature of adsorption process. According to these results, it could be said that the adsorption of B3R dye on pumice decreased over the solution temperature of 40˚C. Therefore, this temperature value was selected as optimum for further experiments.

Langmuir, Freundlich and Temkin isotherm model plots for 40˚C are given in Fig. 6(a)–(c), respectively.

3.1.5. Kinetic studies

In order to specify the mechanism of sorption and to optimize the different operating conditions for the adsorption of B3R onto pumice, kinetic studies were performed using pseudo-first-order and pseudo-second-order kinetic models. These kinetic models were evaluated according to the level of correlation coefficient of R^2.

Table 2
Isotherm parameters for B3R adsorption on to the pumice stone

		Langmuir isotherm			Freundlich isotherm			Temkin isotherm			
T (˚C)	m (g)	q_m	b	R^2	K_F	n	R^2	A	B	b_T	R^2
25	1	48.577	0.088	0.941	4.378	1.521	0.948	0.577	15.632	169.060	0.890
	5	22.613	0.037	0.970	0.764	1.078	0.970	0.483	5.350	486.44	0.835
	10	16.805	0.026	0.985	0.833	1.061	0.985	0.516	5.598	464.87	0.870
30	1	64.497	0.058	0.964	4.102	1.364	0.961	0.498	18.148	143.39	0.906
	5	54.840	0.013	0.986	0.693	1.018	0.983	0.454	5.765	451.183	0.873
	10	38.593	0.011	0.989	0.819	1.020	0.982	0.511	5.937	438.32	0.894
35	1	85.382	0.058	0.978	5.380	1.340	0.964	0.630	20.713	128.645	0.924
	5	64.709	0.016	0.987	0.970	1.011	0.983	0.593	6.192	420.26	0.878
	10	57.253	0.010	0.986	1.115	1.009	0.974	0.661	6.389	407.31	0.892
40	1	97.58	0.074	0.994	7.037	1.303	0.999	0.816	23.428	111.08	0.911
	5	70.49	0.021	0.996	1.703	1.285	0.962	0.954	5.085	511.718	0.980
	10	64.68	0.012	0.986	1.884	1.335	0.949	1.062	4.970	523.58	0.993
45	1	74.613	0.077	0.966	5.712	1.366	0.956	0.687	20.612	126.159	0.904
	5	29.148	0.039	0.987	1.188	1.206	0.972	0.681	5.064	513.87	0.926
	10	22.471	0.030	0.998	1.457	1.221	0.981	0.819	5.237	496.93	0.957

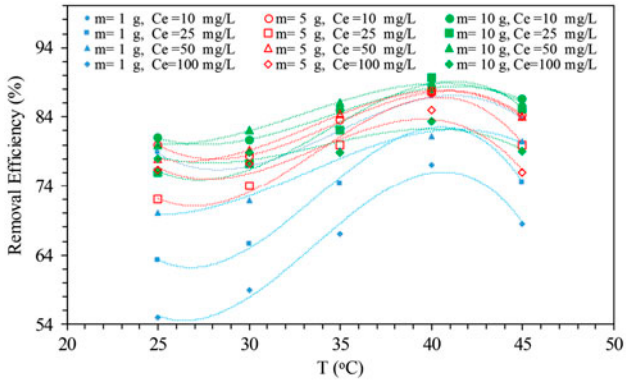

Fig. 5. Effect of temperature on adsorption efficiency (pH 12, shaking speed = 200 rpm).

Linear forms of these models are given in Eqs. (8) and (9) [33]:

$$\log(q_e - q_t) = \log q_e - \frac{k_1}{2.303}t \tag{8}$$

$$\frac{t}{q_t} = \frac{1}{k_2 q_e^2} + \frac{1}{q_e}t \tag{9}$$

where k_1 (1/min) and k_2 (g/mg min) are the adsorption rate constants of first-order and second-order kinetic models, respectively, q_e (mg/g) is the equilibrium adsorption uptake and q_t (mg/g) is the adsorption uptake at the t time. k_1 and k_2 were calculated from the slope and the intercept of $\log(q_e - q_t)$ vs. t (Fig. 7(a)) and t/q_t vs. t (Fig. 7(b)) plots, respectively.

Root mean square errors (RMSE) were also determined to measure the differences between the experimental ($q_{e,exp}$) and predicted ($q_{e,cal}$) values of the kinetic models at the end of the n number of the experiments. The RMSE equation is given in Eq. (10):

$$\text{RMSE} = \sqrt{\frac{\sum_{i=1}^{n}(q_{e,exp} - q_{e,cal})^2}{n}} \tag{10}$$

Table 3 represents the entire kinetics parameters of pseudo-first and second-order models for the adsorption of B3R dye onto pumice. As seen from Table 3, the experimental $q_{e,exp}$ values of the pseudo-second-order model are closer to the predicted $q_{e,cal}$ values, and R^2 correlation coefficients are bigger for all conditions than those of the pseudo-first-order kinetic model. In addition, the other model parameters (k_1, k_2 and RMSE) are more favourable in the pseudo-second-order kinetic model (Table 3) which indicate that the adsorption of B3R dye on to the pumice stone process is controlled by chemisorption [33]. It is also easily seen from Table 3 that k_2 rate constants of pseudo-second-order kinetic model, decrease with initial dye concentrations and increase with adsorbent concentrations. This behaviour can be explained that lower B3R dye and higher pumice stone concentrations exhibit less competition at the adsorbate surface.

Adsorption processes usually consist of more than one steps such as film or boundary layer diffusion, particle or intraparticle diffusion and sorption. The intraparticle mass-transfer diffusion model given below is applied to clarify the diffusion mechanism [37]:

$$q_t = k_i t^{1/2} + C \tag{11}$$

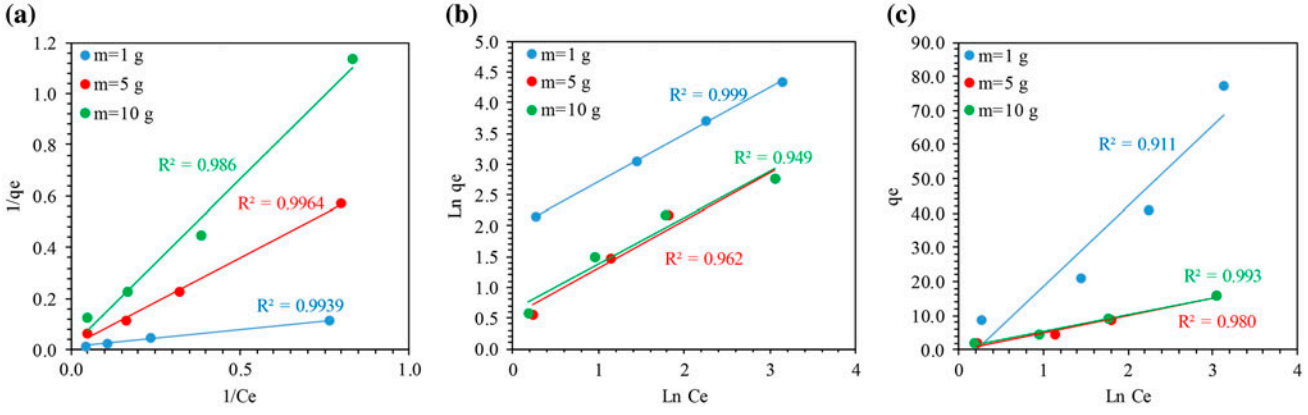

Fig. 6. Langmuir (a), Freundlich (b) and Temkin (c) isotherm model plots (temperature = 40°C, pH 12, shaking speed = 200 rpm).

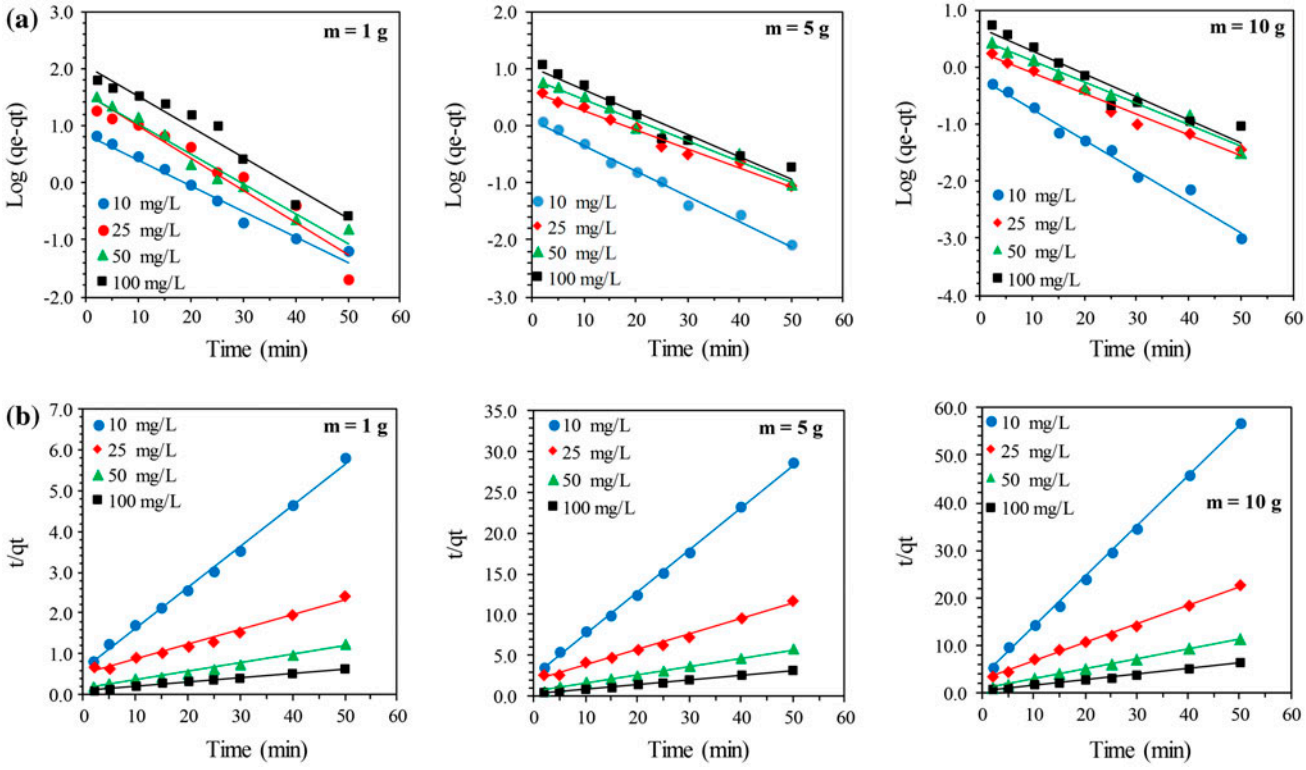

Fig. 7. Pseudo-first- (a) and second- (b) order kinetic models (temperature = 40°C, pH 12, shaking speed = 200 rpm).

where k_i (mg/g min$^{0.5}$) is the intraparticle diffusion rate constant and C (mg/g) describes the boundary layer thickness. k_i and C are the slope and intercept of the q_t vs. $t^{1/2}$ plot, respectively.

The constants of intraparticle diffusion model are given in Table 3. As seen from this table, the values of intercept C, relating to the thickness of the boundary layer, are not equal to zero. Since the thickness of the boundary layer increase with increasing adsorbate concentration, higher values of C obtained at higher B3R dye and lower pumice stone concentrations. As a result, higher C values at higher dye concentrations and relatively poor R^2 values of intraparticle diffusion model (Table 3) proves that the adsorption process of B3R dye on to the pumice stone is not only depended on intraparticle diffusion but other mechanisms might be involved.

3.2. Continuous mode (column) studies

Even though some useful and important data can be obtained with batch mode adsorption studies, continuous mode studies usually serve more practical results for real applications. From this point of view, column mode adsorption experiments initialised after the batch mode studies accomplished, in the present study. Moreover, some batch experimental parameters, such as n value of Freundlich isotherm for Clark model or optimum temperature and pH, etc. are usually required for column studies.

3.2.1. Breakthrough curves

Since the shape of the breakthrough curve and required time for the appearance of breakthrough are important to evaluate an adsorption column, C_t/C_o vs. time plots for different initial dye concentrations, flow rates and bed heights were formed at Fig. 8(a)–(c), respectively.

where C_o and C_t are the dye concentrations (mg/L) at initial and t time, respectively.

The effect of initial dye concentration was investigated by varying the concentration of B3R solution from 10 to 200 mg/L at a constant pumice bed height of 20 cm and flow rate of 2.0 mL/min. C_t/C_o vs. time curves for different initial dye concentrations are shown in Fig. 8(a). As seen from this figure, time to attain 50% capacity of breakthrough decreased with increasing initial dye concentration because the adsorbent binding sites are quickly saturated by B3R dye.

Table 3
Pseudo-first- and second-order kinetic and intraparticle diffusion model results

			Pseudo-first-order model					Pseudo-second-order model					Intraparticle diffusion model		
m (g)	C_o (mg/L)	$q_{e,exp}$ (mg/g)	k_1	R^2	$q_{e,cal}$	RMSE	$\lvert q_{e,exp} - q_{e,cal} \rvert$	k_2	R^2	$q_{e,cal}$	RMSE	$\lvert q_{e,exp} - q_{e,cal} \rvert$	k_i	C	R^2
1	10	8.69	0.104	0.978	7.12	19.798	1.56	0.018	0.997	9.69	8.12	1.00	0.967	1.913	0.823
	25	20.8	0.130	0.941	36.11		15.33	0.003	0.986	23.20		2.44	2.867	2.460	0.880
	50	40.6	0.120	0.970	34.69		5.91	0.004	0.994	42.77		2.17	4.698	10.850	0.785
	100	77.0	0.123	0.958	112.99		35.99	0.001	0.995	81.37		4.37	9.792	12.118	0.901
5	10	1.75	0.102	0.985	1.25	2.901	0.50	0.121	0.999	1.90	0.997	0.15	0.174	0.630	0.794
	25	4.38	0.077	0.982	3.88		0.50	0.019	0.995	5.18		0.80	0.553	0.663	0.887
	50	8.78	0.084	0.981	6.60		2.18	0.018	0.998	9.66		0.88	0.916	2.698	0.868
	100	15.76	0.090	0.951	10.43		5.33	0.011	0.998	17.35		1.59	1.684	4.902	0.808
10	10	0.88	0.124	0.985	0.64	1.736	0.24	0.348	0.999	0.94	0.395	0.06	0.076	0.398	0.762
	25	2.24	0.084	0.971	1.82		0.41	0.056	0.997	2.53		0.29	0.257	0.531	0.876
	50	4.41	0.085	0.978	2.96		1.45	0.051	0.999	4.72		0.31	0.396	1.777	0.860
	100	7.89	0.092	0.932	4.77		3.11	0.027	0.998	8.55		0.66	0.785	2.849	0.801

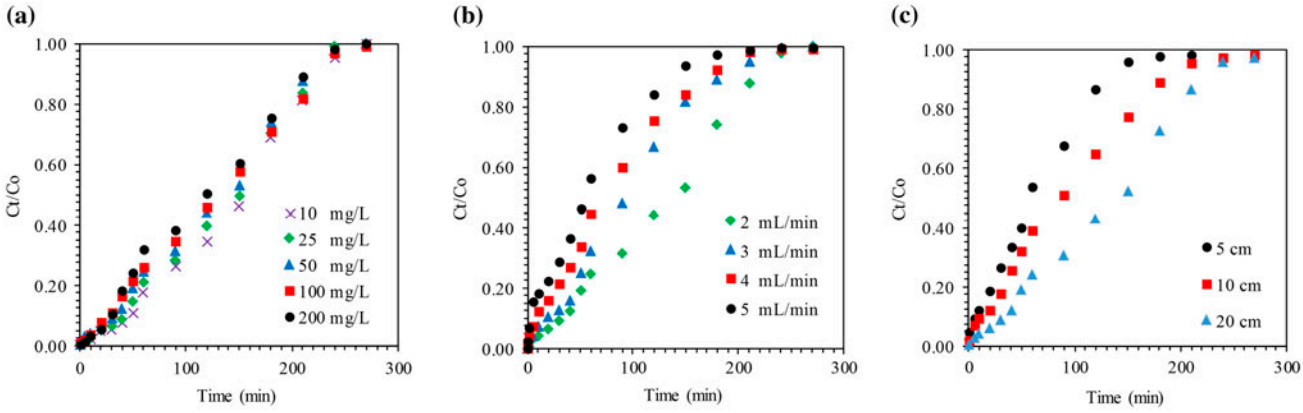

Fig. 8. Breakthrough curves of B3R through the pumice bed at different initial dye concentration (a), flow rate (b) and bed heights (c) (pH 12 and temperature = 40°C).

In addition, the lower concentration gradient causes slower transport rate due to a decreasing diffusion coefficient or decreasing mass transfer coefficient [25]. Sharper breakthrough curves were observed with higher inlet B3R concentration. When the lowest B3R concentration (10 mg/L) was applied, a delayed breakthrough curve was observed (Fig. 8(a)) since the lower concentration gradient causes reduced transport of dye. The driving force for adsorption is the concentration difference between the solute on the adsorbent and the solute in the solution. Sharper breakthrough curves indicate shortened mass transfer zones with higher adsorption rates. As a result, if quick dye uptake is desired, higher initial dye concentrations shall be applied [4].

Likewise, the effect of column inflow rate was investigated by varying the inflow rate of B3R solution from 2 to 5 mL/min at a constant pumice bed height of 20 cm and initial dye concentration of 50 mg/L. C_t/C_o vs. time curves for different inflow rates are shown in Fig. 8(b). As seen from this figure, the steepness of breakthrough curves increased with increasing column inflow rate and adsorption was rapid at the beginning for all flow rates. This can be explained by the availability of free reaction sites around or inside the pumice particles at the beginning of the experiments. Afterwards, dye uptakes become less effective when these sites filled with B3R dye. The breakthrough times and adsorbed amount of B3R dye decreased when the flow rate increased. Although B3R adsorption on to pumice was relatively fast in batch mode or at lower flow rates, residence times were inadequate for completion of entire adsorption at higher flow rates. As a result, lower flow rates can be accepted as favourable for the effective removal of B3R in column mode.

The breakthrough curves of B3R adsorption onto pumice at different bed heights (5, 10 and 20 cm), at constant flow rate of 2.0 mL/min and at initial dye concentration of 50 mg/L are shown in Fig. 8(c). As expected, the breakthrough curves reached the saturated point (the point at which $C_t/C_o = 0.95$) more slowly at the bed height of 20 cm. The slope of the breakthrough curve decreased with increasing bed height (Fig. 8(c)), which resulted in a broadened mass transfer zone [42].

3.2.2. Application of breakthrough curve models

In the present study, Thomas and Clark mathematical models were used to describe the column breakthrough curves for different bed heights, flow rates and dye concentrations.

Thomas model is one of the most general and widely used methods in the column performance theory [43], and assumes plug flow behaviour in the column bed. The linearized form of this model is given in Eq. (12) [44]:

$$\ln\left(\frac{C_o}{C_t} - 1\right) = \frac{k_{Th} q_o m}{Q} - k_{Th} C_o t \tag{12}$$

where k_{Th} is the constant of Thomas model (mL/min mg), q_o is the adsorption capacity (mg/g), and t is the total flow time (min). The values of k_{Th} and q_o can be determined from the slope and intercept of the $\ln((C_o/C_t) - 1)$ vs. t plot, respectively.

In addition to the Thomas model parameters of k_{Th} and q_o, some of error analysis methods such as sum of square error (SSE), sum of absolute error (SAE), average relative error (ARE) and average relative standard

error (ARS) were used to verify the degree of matching of the column adsorption models to the experimental data. The expressions for these error functions are given below [45]:

$$\mathrm{SSE} = \sum_{i=1}^{n} \left(q_{\mathrm{cal}} - q_{\mathrm{exp}}\right)_i^2 \tag{13}$$

$$\mathrm{SAE} = \sum_{i=1}^{n} \left|q_{\mathrm{cal}} - q_{\mathrm{exp}}\right|_i \tag{14}$$

$$\mathrm{ARE} = \frac{1}{n}\sum_{i=1}^{n} \left|\frac{q_{\mathrm{cal}} - q_{\mathrm{exp}}}{q_{\mathrm{exp}}}\right| \tag{15}$$

$$\mathrm{ARS} = \sqrt{\frac{\sum_{i=1}^{n}\left[\frac{q_{\mathrm{cal}} - q_{\mathrm{exp}}}{q_{\mathrm{exp}}}\right]^2}{n-1}} \tag{16}$$

Clark model combines the Freundlich equation with the mass transfer concept and incorporates the parameter n of the Freundlich adsorption isotherm [46]. The linearized form of this model is given below [47]:

$$\ln\left[\left(\frac{C_o}{C_t}\right)^{n-1}\right] = \ln A - r\,t \tag{17}$$

where n is the Freundlich constant and both r and A are the Clark constants. r and A can be determined from the slope and intercept of the $\ln(C_o/C_t)^{n-1}$ vs. time plot, respectively.

Thomas and Clark model results are given in Tables 4 and 5, respectively, for different dye concentrations (C_o), flow rates (Q) and pumice bed heights (Z).

As seen from Table 4, k_{Th} values decreased with increasing initial B3R concentration and pumice bed depth and decreasing flow rate. On the other hand, q_o values decreased with increasing flow rate and pumice bed depth but increased with increasing initial B3R concentration. Similar observations have been reported by other researchers [48].

According to the Thomas model error analysis parameters (Table 4), best results were obtained with 50 mg/L of initial B3R solution concentration and 20 cm of pumice bed height. The correlation coefficients of R^2 at this operating conditions are greater than 0.94. In addition, SSE, SAE, ARE and ARS were observed more favourable than the others. The best SSE value is obtained as 0.67 for 50 mg/L of C_o, 4 mL/min of Q and 20 cm of bed height. As it is well known, lower SSE values indicate the model is more favourable.

Clark model was tested for three different n constant of Freundlich (Table 2, 40˚C). n_1, n_5 and n_{10} are the calculated n values of 1, 5 and 10 g of pumice, respectively. Model results are given in Table 5. The maximum adsorption capacity related to Thomas model was found to be 44.41 mg/g at flow rate of 2 mL/min, dye concentration of 200 mg/L, pH 12 and bed height of 20 cm.

From Table 5, it can be said that, the value of A generally decreases with increasing initial B3R concentration, flow rate and pumice bed depth. On the other hand, the value of r nearly stabile with B3R concentration but increases with increasing flow rate and decreasing pumice bed depth, in most cases. Bigger correlation coefficients (R^2) for smaller C_o values and higher flow rates, suggest the heterogeneous adsorption. In contrast, the adsorbate molecules become homogeneously distributed on the surface of adsor-

Table 4
Thomas model parameters for different conditions

C_o	Q	Z	k_{Th}	q_o	R^2	SSE	SAE	ARE	ARS
10	2	20	0.0184	2.75	0.922	32.13	17.42	1.38	1.54
25	2	20	0.0077	6.48	0.908	45.84	19.92	3.15	6.47
50	2	20	0.0038	12.27	0.946	3.09	4.62	0.52	0.92
100	2	20	0.0019	23.40	0.832	42.67	19.29	2.17	2.93
200	2	20	0.0011	44.41	0.803	49.49	21.63	5.58	12.17
50	3	20	0.0056	5.26	0.970	1.31	2.96	0.50	0.95
50	4	20	0.0089	2.51	0.983	0.67	2.06	0.14	0.17
50	5	20	0.0394	0.53	0.940	39.02	18.55	13.48	38.89
50	2	10	0.0054	13.50	0.892	45.67	20.80	4.23	6.06
50	2	5	0.0088	14.57	0.877	63.87	23.57	10.39	23.54

Table 5
Clark model parameters for different conditions

			n_1 = 1.303[a]			n_5 = 1.285[a]			n_{10} = 1.335[a]		
C_o	Q	Z	A	r	R^2	A	r	R^2	A	r	R^2
10	2	20	2.295	0.016	0.964	2.072	0.015	0.966	2.717	0.016	0.962
25	2	20	2.245	0.017	0.949	2.029	0.016	0.951	2.656	0.017	0.946
50	2	20	1.970	0.017	0.901	1.785	0.016	0.904	2.319	0.017	0.896
100	2	20	1.901	0.017	0.911	1.724	0.017	0.913	2.234	0.018	0.907
200	2	20	2.071	0.019	0.888	1.873	0.019	0.891	2.444	0.020	0.883
50	3	20	1.706	0.022	0.991	1.557	0.022	0.991	1.983	0.023	0.990
50	4	20	1.261	0.023	0.982	1.157	0.023	0.983	1.454	0.023	0.980
50	5	20	1.020	0.028	0.960	0.938	0.027	0.960	1.170	0.028	0.959
50	2	10	1.386	0.021	0.942	1.267	0.021	0.944	1.606	0.022	0.939
50	2	5	1.201	0.027	0.978	1.102	0.027	0.979	1.383	0.028	0.977

[a]Freundlich isotherm n values.

bent when the slower flow rates applied [49]. Maximal R^2 value of Thomas model was observed as 0.991 at 3 mL/min flow rate, 50 mg/L dye concentration, pH 12 and 20 cm bed height conditions. As a result, as can be seen from Tables 4 and 5, the correlation coefficients of Clark model are usually more favourable than those of Thomas.

3.3. FTIR spectrum of pumice

The chemical composition of pumice used in this study as weight % is SiO_2 72.07, AlO_2 13.50, K_2O 11.27, Na_2O 1.60, Fe_2O_3 1.21 and TiO_2 0.35. As is also understood from these values, SiO_2 and AlO_2 are the two main components of the pumice. Fig. 9 shows the

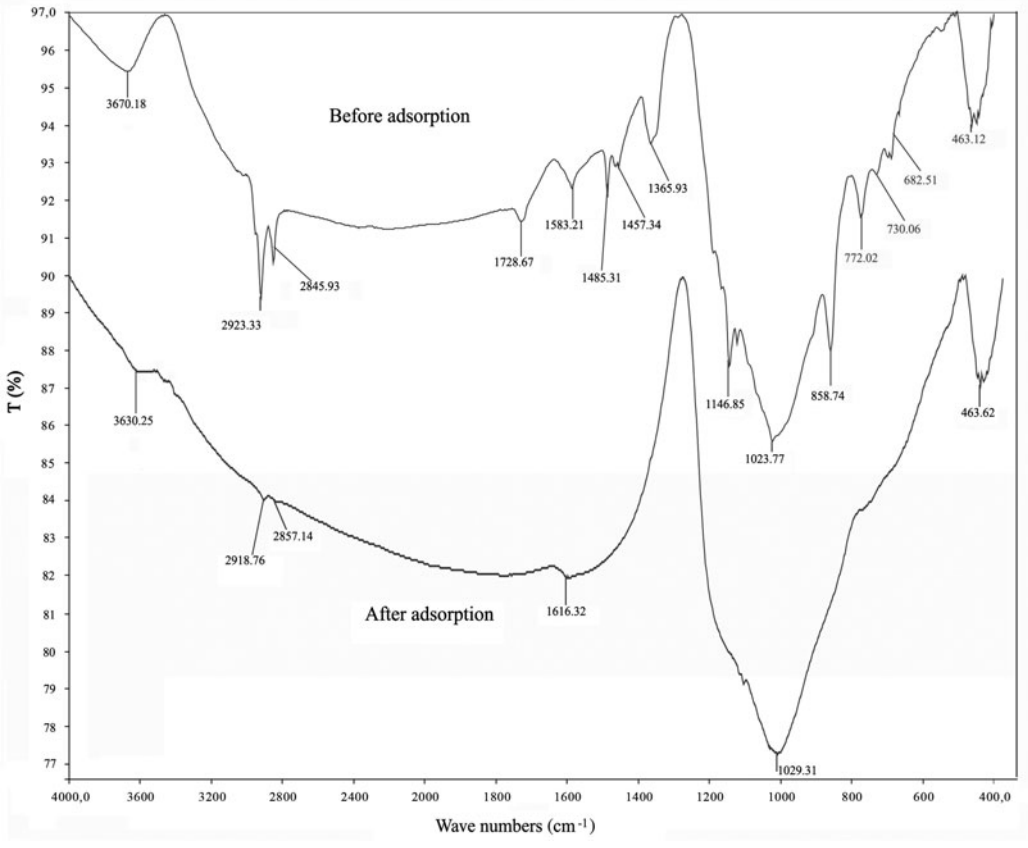

Fig. 9. FTIR spectrum of pumice granules before and after adsorption.

Fourier transform infrared spectroscopy (FTIR) of the pumice before and after adsorption at wavelengths ranging from 400 to 4,000 cm^{-1}. The peaks at 463.12 and 858.74 cm^{-1} were resulted from the Si–O bending strength vibrations of the amorphous quartz. The strong peaks between 1,000 and 1,150 cm^{-1} may have resulted from Si–O stretching vibrations [50]. For SiO_2 and AlO_2 bonds, the characteristic stretching vibrations were detected at the wave number of 1,023.77 cm^{-1}. The small peak at 682.51 cm^{-1} can be assigned to the regional vibration of reductive carbon in the crystal lattice [28]. Other peaks can be assigned to the adsorbed water molecules including the broadening peak at 3,670.18 cm^{-1} that belongs to the asymmetric stretching vibration of H–O bond. This shows OH group on the surface.

Nearly all of the peaks in the spectroscopy of pumice for before and after adsorption have similar shapes but different wavenumbers. In addition, some peaks are disappeared or shifted and a few new peaks are detected. This indicates the possible bindings of functional groups on the surface of the pumice. The intensities and wavenumber of peaks were either reduced or slightly shifted after adsorption. This can be resulted from electrostatic interactions between the positively charged functional groups.

4. Conclusion

The removal of B3R dye over pumice has been investigated in the present study. Pumice exhibited favourable adsorption capacity to remove B3R dye from aqueous solutions in batch and continuous mode. Langmuir, Freundlich and Temkin isotherm models were tested in the batch mode of study. According to the results, Langmuir is more favourable isotherm model then the others (Table 2). The validity of isotherm models based on the correlation values is in the following order: Langmuir > Freundlich > Temkin. The maximum uptake capacity, q_m, is determined as 95.78 mg/g for 10 g of pumice quantity, 40°C and pH 12. As seen from the isotherm models tested in this study, 40°C have more favourable results than lower or upper temperature values. At higher temperatures, the exothermic nature of adsorption process and the weak bonds between dye molecules and binding sites of pumice can explain this situation. The batch kinetic study indicated that the adsorption of B3R dye on to pumice could be well fitted by the pseudo-second-order equation. The lowest RMSE value of 0.395 was observed at pseudo-second-order kinetic model for 10 g of pumice (Table 3).

It can be seen from the column studies data, the uptake of B3R dye in a fixed-bed pumice column depends on pumice bed depth, influent B3R dye solution concentration and flow rates. Both of the Thomas and Clark models produced acceptable results for designing an adsorption column, but Clark model seemed more sensitive. According to the results of Thomas and Clark models, removal rates of B3R dye in a fixed-bed pumice adsorption column could be higher at lower flow rates and higher pumice bed heights.

Consequently, pumice stone could be considered as an effective adsorbent that can be utilized in an adsorption column for the removal of B3R dye from aqueous solution. Furthermore, mathematical modelling of the adsorption dynamic under continuous flow conditions could provide important parameters for real applications [51].

References

[1] G. Crini, Non-conventional low-cost adsorbents for dye removal: A review, Bioresour. Technol. 97 (2006) 1061–1085.
[2] J. Mittal, D. Jhare, H. Vardhan, A. Mittal, Utilization of bottom ash as a low-cost sorbent for the removal and recovery of a toxic halogen containing dye eosin yellow, Desalin. Water Treat. 52 (2014) 4508–4519.
[3] W. Zhang, F. Liang, C. Li, L. Qiu, Y. Yuan, F. Peng, X. Jiang, A. Xie, Y. Shen, J. Zhu, Microwave-enhanced synthesis of magnetic porous covalent triazine-based framework composites for fast separation of organic dye from aqueous solution, J. Hazard. Mater. 186 (2011) 984–990.
[4] J. Song, W. Zou, Y. Bian, F. Su, R. Han, Adsorption characteristics of methylene blue by peanut husk in batch and column modes, Desalination 265 (2011) 119–125.
[5] J. de Jesus da Silveira Neta, G. Costa Moreira, C. Juliano da Silva, C. Reis, E. Lázaro Reis, Use of polyurethane foams for the removal of the Direct Red 80 and Reactive Blue 21 dyes in aqueous medium, Desalination 281 (2011) 55–60.
[6] J. Sun, S. Sun, G. Wang, L. Qiao, Degradation of azo dye Amido black 10B in aqueous solution by Fenton oxidation process, Dyes Pigm. 74 (2007) 647–652.
[7] X. Zhu, Y. Zheng, Z. Chen, Q. Chen B. Gao, S. Yu, Removal of reactive dye from textile effluent through submerged filtration using hollow fiber composite nanofiltlration membrane, Desalin. Water Treat. 51 (2013) 6101–6109.
[8] H. Jirankova, J. Mrazek, P. Dolecek, J. Cakl, Organic dye removal by combined adsorption–membrane separation process, Desalin. Water Treat. 20 (2010) 96–101.
[9] M. Rafatullah, O. Sulaiman, R. Hashim, A. Ahmad, Adsorption of methylene blue on low-cost adsorbents: A review, J. Hazard. Mater. 177 (2010) 70–80.
[10] J.W. Lee, S.P. Choi, R. Thiruvenkatachari, W.G. Shim, H. Moon, Evaluation of the performance of adsorption and coagulation processes for the maximum removal of reactive dyes, Dyes Pigm. 69 (2006) 196–203.

[11] F.I. Hai, K. Yamamoto, K. Fukushi, Hybrid treatment systems for dye wastewater, Crit. Rev. Environ. Sci. Technol. 37 (2007) 315–377.
[12] M. Dükkancı, G. Gündüz, S. Yılmaz, R.V. Prihod'ko, Heterogeneous Fenton-like degradation of Rhodamine 6G in water using CuFeZSM-5 zeolite catalyst prepared by hydrothermal synthesis, J. Hazard. Mater. 181 (2010) 343–350.
[13] X.C. Ruan, M.Y. Liu, Q.F. Zeng, Y.H. Ding, Degradation and decolorization of reactive red X-3B aqueous solution by ozone integrated with internal micro-electrolysis, Sep. Purif. Technol. 74 (2010) 195–201.
[14] H.N. Bhatti, Y. Safa, Removal of anionic dyes by rice milling waste from synthetic effluents: Equilibrium and thermodynamic studies, Desalin. Water Treat. 48 (2012) 267–277.
[15] F.A. Khari, M. Khatibzadeh, N.M. Mahmoodi, K. Gharanjig, Removal of anionic dyes from aqueous solution by modified alginate, Desalin. Water Treat. 51 (2013) 2253–2260.
[16] C.H. Liu, J.S. Wu, H.C. Chiu, S.Y. Suen, K.H. Chu, Removal of anionic reactive dyes from water using anion exchange membranes as adsorbers, Water Res. 41 (2007) 1491–1500.
[17] J.S. Wu, C.H. Liu, K.H. Chu, S.Y. Suen, Removal of cationic dye methyl violet 2B from water by cation exchange membranes, J. Membr. Sci. 309 (2008) 239–245.
[18] A.G. Espantaleón, J.A. Nieto, M. Fernandez, A. Marsal, Use of activated clays in the removal of dyes and surfactants from tannery waste waters, Appl. Clay Sci. 24 (2003) 105–110.
[19] A.S. Özcan, B. Erdem, A. Özcan, Adsorption of Acid Blue 193 from aqueous solutions onto Na–bentonite and DTMA–bentonite, J. Colloid Interface Sci. 280 (2004) 44–54.
[20] M. Özacar, I.A. Şengil, Adsorption of metal complex dyes from aqueous solutions by pine sawdust, Bioresour. Technol. 96 (2005) 791–795.
[21] X. Zhang, A. Li, Z. Jiang, Q. Zhang, Adsorption of dyes and phenol from water on resin adsorbents: Effect of adsorbate size and pore size distribution, J. Hazard. Mater. 137 (2006) 1115–1122.
[22] M. Chiou, H.-Y. Li, Equilibrium and kinetic modeling of adsorption of reactive dye on cross-linked chitosan beads, J. Hazard. Mater. 93 (2002) 233–248.
[23] V.K. Garg, M. Amita, R. Kumar, R. Gupta, Basic dye (methylene blue) removal from simulated wastewater by adsorption using Indian Rosewood sawdust: A timber industry waste, Dyes Pigm. 63 (2004) 243–250.
[24] A. Mittal, V. Thakur, J. Mittal, H. Vardhan, Process development for the removal of hazardous anionic azo dye Congo red from wastewater by using hen feather as potential adsorbent, Desalin. Water Treat. 52 (2014) 227–237.
[25] M.T. Uddin, M. Rukanuzzaman, M.M. Rahman Khan, M.A. Islam, Adsorption of methylene blue from aqueous solution by jackfruit (Artocarpus heteropyllus) leaf powder: A fixed-bed column study, J. Environ. Manage. 90 (2009) 3443–3450.
[26] M. Tapan, Z. Yalçın, O. İçelli, H. Kara, S. Orak, A. Özvan, T. Depci, Effect of physical, chemical and electro-kinetic properties of pumice samples on radiation shielding properties of pumice material, Ann. Nucl. Energy 65 (2014) 290–298.
[27] P. Rashiddadash, A.A. Ramezanianpour, M. Mahdikhani, Experimental investigation on flexural toughness of hybrid fiber reinforced concrete (HFRC) containing metakaolin and pumice, Constr. Build. Mater. 51 (2014) 313–320.
[28] M.N. Sepehr, M. Zarrabi, H. Kazemian, A. Amrane, K. Yaghmaian, H.R. Ghaffari, Removal of hardness agents, calcium and magnesium, by natural and alkaline modified pumice stones in single and binary systems, Appl. Surf. Sci. 274 (2013) 295–305.
[29] R. Akkaya, Uranium and thorium adsorption from aqueous solution using a novel polyhydroxyethylmethacrylate-pumice composite, J. Environ. Radioact. 120 (2013) 58–63.
[30] N.G. Turan, B. Mesci, O. Ozgonenel, The use of artificial neural networks (ANN) for modeling of adsorption of Cu(II) from industrial leachate by pumice, Chem. Eng. J. 171 (2011) 1091–1097.
[31] F. Gode, E. Moral, Column study on the adsorption of Cr(III) and Cr(VI) using Pumice, Yarıkkaya brown coal, Chelex-100 and Lewatit MP 62, Bioresour. Technol. 99 (2008) 1981–1991.
[32] K.A. Karimaian, A. Amrane, H. Kazemian, R. Panahi, M. Zarrabi, Retention of phosphorous ions on natural and engineered waste pumice: Characterization, equilibrium, competing ions, regeneration, kinetic, equilibrium and thermodynamic study, Appl. Surf. Sci. 284 (2013) 419–431.
[33] G. Asgari, B. Roshani, G. Ghanizadeh, The investigation of kinetic and isotherm of fluoride adsorption onto functionalize pumice stone, J. Hazard. Mater. 217–218 (2012) 123–132.
[34] F. Akbal, Adsorption of basic dyes from aqueous solution onto pumice powder, J. Colloid Interface Sci. 286 (2005) 455–458.
[35] E.V. Veliev, T. Öztürk, S. Veli, A.G. Fatullayev, Application of diffusion model for adsorption of azo reactive dye on pumice, Polish J. Environ. Stud. 15 (2006) 347–353.
[36] U. Filipkowska, E. Klimiuk, S. Grabowski, E. Siedlecka, Adsorption of reactive dyes by modified chitin from aqueous solutions, Polish J. Environ. Stud. 11 (2002) 315–323.
[37] P. Wang, Q. Ma, D. Hu, L. Wang, Adsorption of methylene blue by a low-cost biosorbent: Citric acid modified peanut shell, Desalin. Water Treat. 57 (2016) 10261–10269.
[38] I. Langmuir, The adsorption of gases on plane surfaces of glass, mica and platinum, J. Am. Chem. Soc. 40 (1918) 1361–1403.
[39] H.M.F. Freundlich, Uber die adsorption in lasungen (Adsorption in solutions), Z. Phys. Chem. 57 (1906) 385–470.
[40] A. Masoumi, M. Ghaemy, Removal of metal ions from water using nanohydrogel tragacanth gum-g-polyamidoxime: Isotherm and kinetic study, Carbohydr. Polym. 108 (2014) 206–215.
[41] S. Sadaf, H.N. Bhatti, S. Ali, K. Rehman, Removal of Indosol Turquoise FBL dye from aqueous solution by bagasse, a low cost agricultural waste: batch and column study, Desalin. Water Treat. 52 (2014) 184–198.
[42] L.W. Low, T.T. Teng, N. Morad, B. Azahari, Optimization of the column studies into the adsorption of basic

dye using tartaric acid-treated bagasse, Desalin. Water Treat. 52 (2014) 6194–6205.
[43] H. Patel, R.T. Vashi, Fixed bed column adsorption of ACID Yellow 17 dye onto tamarind seed powder, Can. J. Chem. Eng. 90 (2012) 180–185.
[44] S. Chen, Q. Yue, B. Gao, Q. Li, X. Xu, K. Fu, Adsorption of hexavalent chromium from aqueous solution by modified corn stalk: A fixed-bed column study, Bioresour. Technol. 113 (2012) 114–120.
[45] S. Chowdhury, P. Saha, Adsorption kinetic modeling of safranin onto rice husk biomatrix using pseudo-first- and pseudo-second-order kinetic models: Comparison of linear and non-linear methods, Clean—Soil, Air, Water 39 (2011) 274–282.
[46] F.A. Batzias, D.K. Sidiras, Dye adsorption by prehydrolysed beech sawdust in batch and fixed-bed systems, Bioresour. Technol. 98 (2007) 1208–1217.
[47] R.M. Clark, Modeling TOC removal by GAC: The general logistic function, J. Am. Water Works Assn. 79 (1987) 33–131.
[48] R. Lakshmipathy, N.C. Sarada, Methylene blue adsorption onto native watermelon rind: Batch and fixed bed column studies, Desalin. Water Treat. 57 (2016) 10632–10645.
[49] M.S. Sajab, C.H. Chia, S. Zakaria, M. Sillanpaa, Fixed-bed column studies for the removal of cationic and anionic dyes by chemically modified oil palm empty fruit bunch fibers: Single- and multisolute systems, Desalin. Water Treat. 55 (2015) 1372–1379.
[50] B. Ersoy, A. Sariisik, S. Dikmen, G. Sariisik, Characterization of acidic pumice and determination of its electrokinetic properties in water, Powder Technol. 197 (2010) 129–135.
[51] A. Šuňovská, V. Hasíková, M. Horník, M. Pipíška, S. Hostin, J. Lesný, Removal of Cd by dried biomass of freshwater moss *Vesicularia dubyana*: Batch and column studies, Desalin. Water Treat. 57 (2016) 2657–2668.